International Journal of New Horizons in Physics

http://dx.doi.org/10.18576/ijnhp/040103

Structural and Magnetic Properties of Diluted Magnetic Semiconducting of $Zn_{1-x}Cr_xO$ Nanocrystalline Powders

M. A. Abdelraheem [1], *M. Mosa*[2], *M. Hassanein* [1]*and A. El-Korashy*[3,*]

[1]Physics Department, Faculty of Science, Assiut University, Assiut, Egypt.
[2]Chemistry Department, Faculty of Science, Banha University, Egypt.
[3]Basic Science Department, Faculty of Engineering, The British University in Egypt, ElShorouk City, Cairo, Egypt.

Received: 21 Feb. 2016, Revised: 28 May 2016, Accepted: 29 May 2016.
Published online: 1 Jan. 2017.

Abstract: Both undoped and Cr doped ZnO nanoparticles with composition of $Zn_{1-x}Cr_xO$ ((x = 0, 0.02, 0.04, 0.06 and 0.08) were prepared by co-precipitation method. These nanoparticles were characterized by using thermogravimetry for identification the calcinations temperature. X-ray diffraction, transition electron microscope, Fourier transform infrared spectroscopy. X-ray diffraction patterns of all the samples displayed peaks of a hexagonal wurzite structure. The structural properties investigated by X-ray diffraction revealed hexagonal wurtzite ZnO type structure. Both XRD and TEM were shown that the crystallite size of the nanoparticle decreases with increasing Cr content. In addition, the magnetic properties as a function of chromium concentrations was studied. $Zn_{1-x}Cr_xO$ ((x = 0.02, 0.04, 0.06 and 0.08) nanoparticles have a ferromagnetic behavior.

Keywords: ZnO nanoparticles, magnetic properties, Transition metals, optoelectronics and spintronics

1 Introduction

Transtion metals with a small fraction doped semiconductors are known as diluted magnetic semiconductors (DMSs) that have potential applications in the field of optoelectronics and spintronics [1, 2]. The diluted magnetic semiconductor (DMS) materials have emerged as a new technological field due to their use in spintronic devices. Spintronic devices like spinvalve transistors, memories, logic device and ultra fast optical switches have encouraged great passions of several researchers for extracted room temperature ferromagnetism in nanostructured ZnO materials [3]. Many efforts have been concentrated on the search for temperature higher than Curie temperature (T_C) ferromagnetism (FM) in transition metal (TM) doped wide banded semiconducting oxides such as TiO_2, ZnO, and SnO_2 [4-9]. Zinc oxide (ZnO) has an important multifunctional II-IV compound semiconductor with a set of properties suitable for a wide range of emerging applications such as optoelectronics, micro/nano electronics, and spintronics devices, bio-medical and catalytic applications.

To integrate these features in an II–VI oxide based semiconducting material, a suitable 3d transition group element has to be modified/replaced in their lattice sites to a certain extent to hold the possibility of dilute magnetic semiconductors (DMS) with a Curie temperature higher than room temperature [10]. Cr is a transition metal element with special abundant electron shells structure and has ionic radius of Cr^{3+} equal 0.063 nm to that of ionic radius Zn^{2+} equal 0.074 nm, which makes easy to emerge into ZnO crystal structure and induce the ferromagnetism at room temperature and enhances the green emission [11]. The theoretical predictions confirm that Cr^{3+} doped ZnO should exhibit stable ferromagnetic material, which is also illustrate in magnetic measurements of Cr^{3+} doped ZnO thin film [12]. Trivalent Cr^{3+} ions exhibit $3d^3$ high-spin configuration, which expect to generate large magnetic moments in the ZnO host semiconductors [13]. In that moment the reported experimental results for Cr^{3+} doped ZnO have been very conflicting. Some studies reveal that magnetic behavior of Cr^{3+}doped ZnO appears to be very sensitive to preparing methods. Ueda et al. [14] and Jin et al. [15] have not observed any ferromagnetic behavior for chromium doped ZnO but some authors [16, 17] have reported room temperature ferromagnetism. In this present work, we synthesized the pure ZnO and and Cr-doped ZnO nanoparticles in terms of precipitation method and used many measurements such as XRD, energy dispersive analysis spectroscopy (EDAS), high-resolution transmission electron microscopy (HRTEM) to verify that Cr^{3+} substitutes for Zn^{2+} in the crystal lattice. Furthermore, the optical and magnetic properties of pure ZnO and Cr-doped ZnO nanoparticles were investigated.

2 Experimental Procedures

All the chemicals used are purchased from Sigma Aldrich (USA) with greater than (99.9%). Both undoped and Cr

*Corresponding author e-mail: amer.el-korashy@bue.edu.eg

doped ZnO nanoparticles with composition of $Zn_{1-x}Cr_xO$ (with $0 \geq x \geq 10$) were prepared by precipitation in methanol. For preparing ZnO, Zinc nitrate hexahydrate [$Zn(NO_3)_2$-$6H_2O$] was dissolved in methanol (100 ml). Both the solutions was mixed by constant magnetic stirring by heating at 60 °C for 4 hour. Filtration was used for separation the precipitation from the solution.

The precipitation was washed more than one time with distilled water and ethanol dried in air at 127 °C to obtain ZnO nanoparticles. For synthesizing Cr-doped ZnO nanoparicles, chromium nitrate tetrahydrate [$Cr(NO_3)_2$-$4H_2O$] with 0.02, 0.04, 0.06 and 0.08 M was added into zinc nitrate hexahydrate with 0.48, 0.46, 0.44 and 0.42 M and the procedure above was repeated. The thermal behavior of the precursor is analyzed by thermogravimetric analysis (TGA) (Shimadzu 50 with an accuracy of ±0.1 K). Finally, the dried samples are grounded and kept for calcination at 480 °C for 2 hours, in order to obtain polycrystalline powder. X-ray diffraction (XRD) Philips X-ray diffractometer (model-X ' pert) with Cu-K□1 radiation (□□= 1.54056 Å) was used for determination the structure phase of pure ZnO and Cr-doped ZnO. Pure silicon (~ 99.9999 %) was used as an internal standard. Transmission electron microscopy (TEM) were carried out by (JEOL-2010) TEM system. The compositional analysis was done by energy dispersive X-ray spectra (EDX). IR absorption measurements were done using Shimadzu FTIR spectrometer through KBr pellet technique. The magnetic properties of pure ZnO and Cr-doped ZnO were studied using the vibrating sample magnetometer model (VSM-9600M-1, USA). The measurements were at room temperature and applied field of 15 kOe.

3 Results and Discussion

In order to determine the calcinations temperature differential scanning colorimetry thermogravimetric analysis (TGA) and its differentiation of the precursor were carried out. The differentiation curve is very important for determination the peaks with a good precision. The specimens were heated from room temperature to 900 °C with an increment of 10 °C/min under nitrogen atmosphere. Fig. 1 shows a plot of TGA and its differentiation. The TGA data shows the weight loss of the precursor which is found to take place until 565 °C. Form the first derivative of TGA curve an exothermic peak at 258 °C and two endothermic peaks are found at 142 °C, 332 °C respectively. These peaks are due to the evaporation of water and organics. A large exothermic peak is exhibited at 482 °C, due to the crystallization of ZnO. Finally, the dried samples are kept calcination temperature at 565 °C for 4 hours for getting nano-crystalline powder.

The elemental compositions of the ZnO and Cr-doped ZnO nanostructures were determined by EDAX measurements. The EDAX analyses were shown the presence of Zn and O peaks (Fig. 1 (a)) for undoped ZnO, while the presence of Cr further ZnO (Fig. 2 (a)) along with Zn and O peaks are evident in the Cr-doped ZnO spectrum. The EDAX results are consistent with the actual atomic percentage of Cr

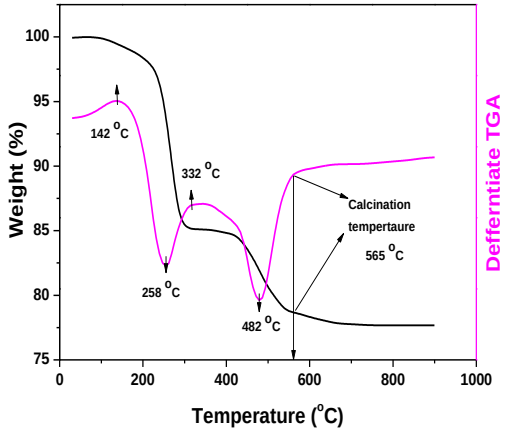

Fig. 1: TGA and its differentiation of ZnO precursor.

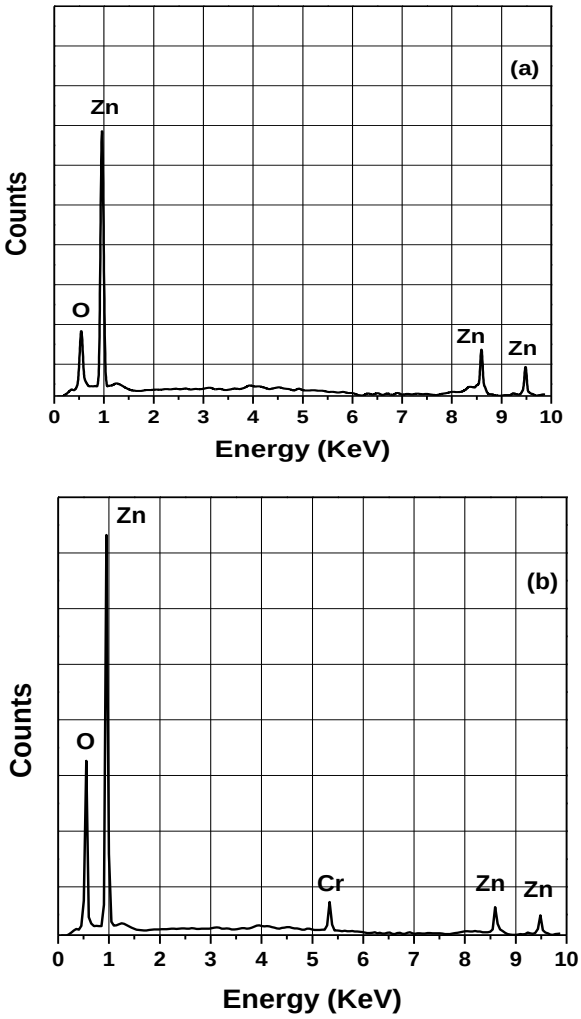

Fig. 2: EDAX spectra of (a) pure ZnO nanoparticles and (b) 8% Cr doped ZnO nanoparticles calcinated at 565 °C for 4 h.

incorporated into ZnO is 7.98 at.% for the sample obtained from 8 % Cr-doped ZnO.

Structural properties of $Zn_{1-x}Cr_xO$ (x = 0.0, 0.02, 0.04, 0.06 and 0.08) were investigated by XRD as shown in Fig. 2. Fig. 2 shows the XRD patterns with distinct peaks, corresponded to the (100), (002), (101), (102), (110), (103), (112) and (201) lattice planes, reveals that as prepared nanoparticles have a wurtizte (hexagonal) structure. This figure also showed that the peaks of ZnO shift towards higher angles with increasing Cr concentration.

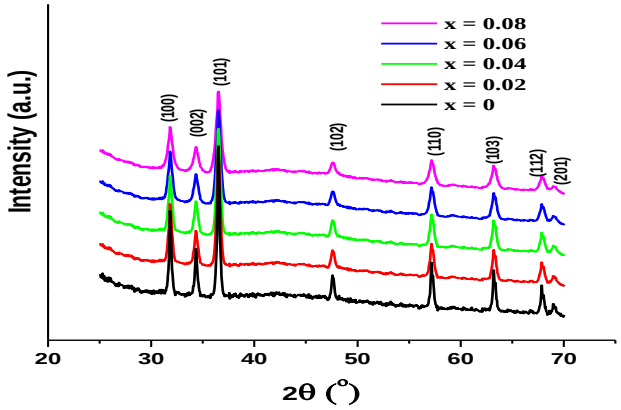

Fig. 3: XRD patterns of $Zn_{1-x}Cr_xO$ (x = 0.0, 0.02, 0.04, 0.06 and 0.08) powders obtained after the calcination at 567 ◦C for 4 h.

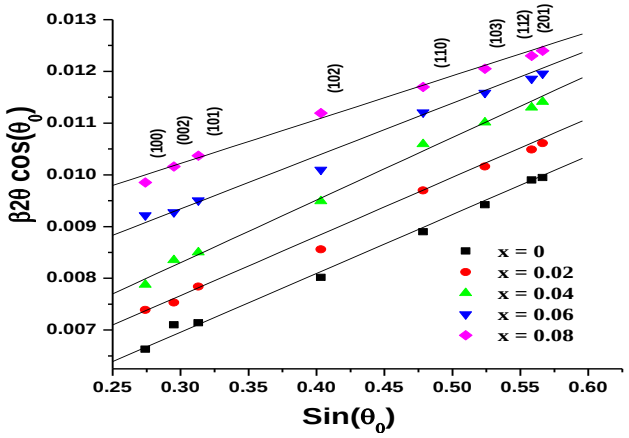

Fig. 4: Crystallite size/lattice strain separation calculating using the FWHM according to "Williamson Hall" method.

This shift may be due to the higher ionic radius of Zn (0.074 nm) as compared to Cr (0.063 nm) ions. The broadening of XRD peaks may be attributed to nano-sized formation of $Zn_{1-x}Cr_xO$ nanoparticles. The reason of peak broadening was due to grain refinement along with the large strain that related with the nanoparticle powders. Peak broadening is due to two evident the **first** is instrumentation effect and the second is microstructure parameters, both crystallite size and lattice strain. By acquiring a diffraction pattern from the line broadening of a standard material (silicon), it is possible to remove the instrumentation effect broadening contribution using the following Eq. [18]:

$$\beta_{hkl}(2\theta) = \sqrt{(\beta_{hkl})^2_{measured} - (\beta_{hkl})^2_{s\tan dard}} \quad (1)$$

Here β_{hkl} is the full width half-maximum (FWHM), which arise from microstructure parameters, both crystallite size broadening, β_c and lattice strain, broadening, β_s:

$$\beta_{hkl} = \beta_c + \beta_s = \frac{k\lambda}{D\cos\theta_0} + 4e(\sin\theta_0) \quad (2)$$

Where D and e are crystallite size and lattice strain, k is shape factor (≈ 0.9), and λ is wavelength of the CuK_α radiation.

Rearranging Eq. (2):

$$\beta_{hkl}\cos\theta_0 = \frac{k\lambda}{D} + 4e(\sin\theta_0) \quad (3)$$

Eq. (3) is the Williamson-Hall(W-H) equations [19].

Fig. 4 displays the plot of $\beta_{hkl}cos(\theta_0)$ vs $sin(\theta_0)$ and the values of e and D can be calculated from the slope and the ordinate intersection respectively. Fig. 4 shows the microstructure parameters of both crystallite size (D) and lattice strain (e) of $Zn_{1-x}Cr_xO$ ($0 \le x \le 0.10$) nanostructures. It is observed that the crystallite size decreases with increasing Cr content but the lattice strain increases. The decrease in crystallite size and increase in lattice strain may be observed due to the replacement of Zn ions by Cr ions.

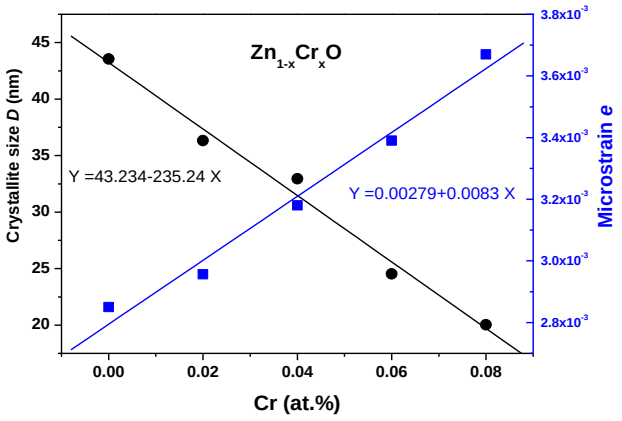

Fig. 5: Crystallize size and lattice strain as a function of Cr content.

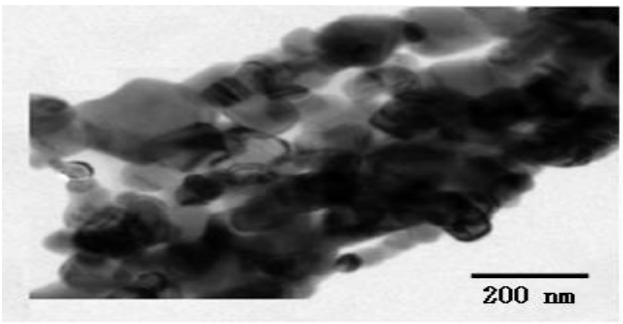

(a)

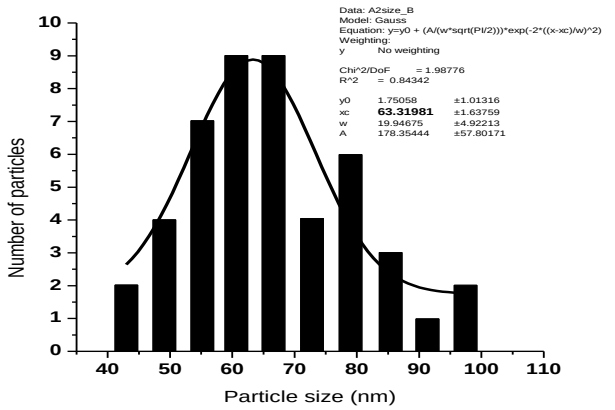

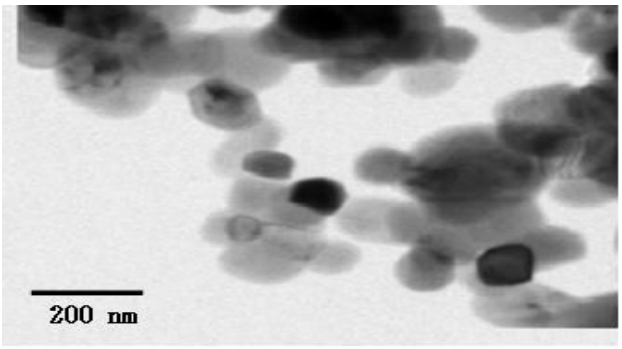

(b)

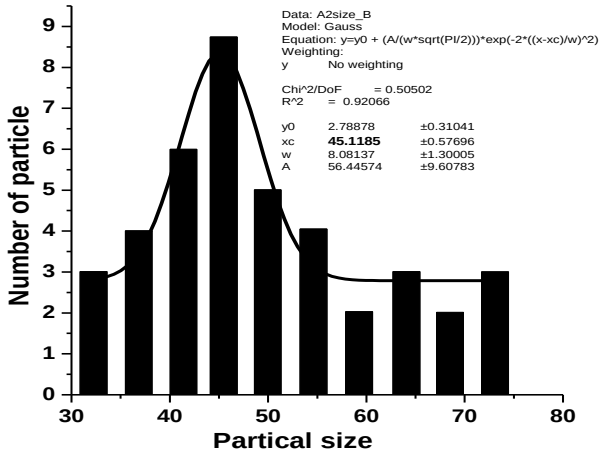

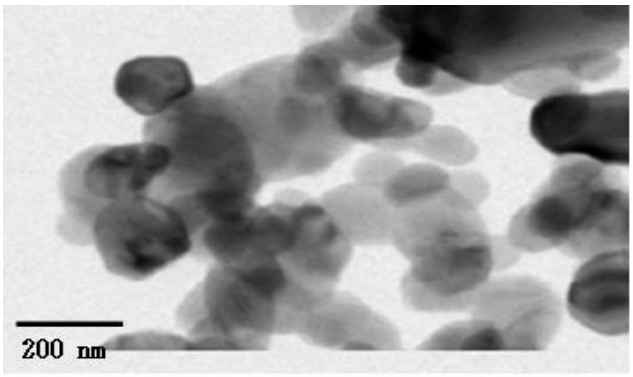

(C)

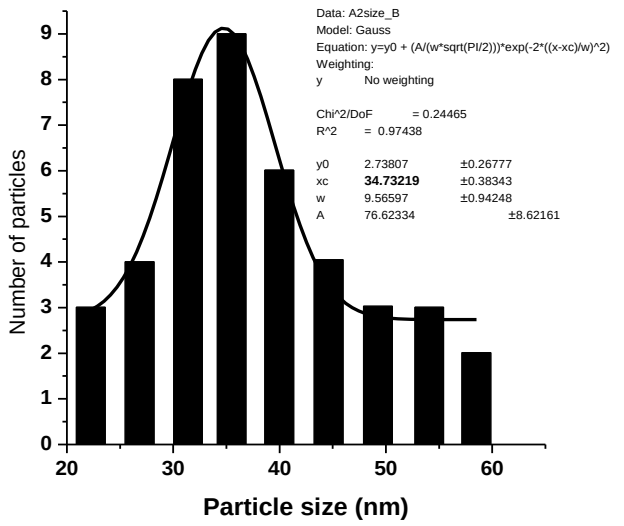

Fig. 6: Representative TEM micrograph of (a) pure ZnO, (b) $Zn_{0.96}Cr_{0.04}O$ and (c) $Zn_{0.96}Cr_{0.04}O$ nanoparticles and their histogram for giving the average size in nm.

Transmission electron microscopy have been used for determination the shape and the particle size of $Zn_{1-x}Cr_xO$ (x = 0.0, 0.04and 0.08) nanoparticles. As seen In Fig. 6 (a-c), all the particles have a spherical shape.

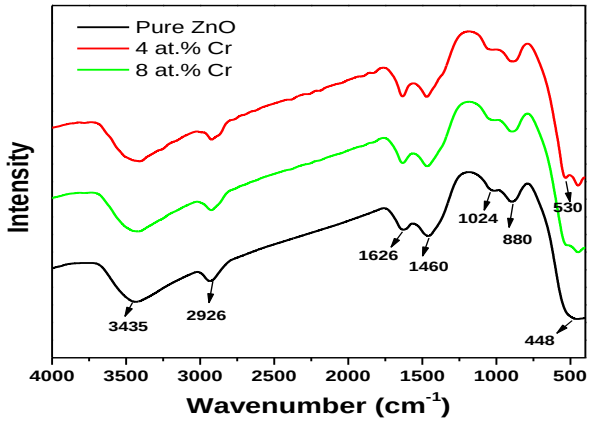

Fig. 7: FTIR spectra of $Zn_{1-x}Cr_xO$ nanoparticles.

The agglomeration is more in pure ZnO but decrease with the Cr doping at Fig 6 (a, c) agglomeration. The average particle sizes of these particles have been calculated in terms of TEM images. For the pure ZnO average particle size was 63.3 nm but Cr doping into ZnO decreases the particle size. The average particle size was 45.1 nm for $Zn_{0.96}Cr_{0.04}O$ and 34.7 nm for $Zn_{0.92}Cr_{0.08}O$ which further decreases with increasing in the Cr concentration. The distribution curve of particle size of $Zn_{1-x}Cr_xO$ (x = 0.0, 0.04and 0.08) is shown in Fig 6 (a, c). The crystallite sizes obtained from the XRD data as shown in Fig. 4 are smaller than the sizes calculated from TEM. It is may be attributed to that the particle size obtained from the XRD data is the crystallite size while TEM gives the particle size that may consist more than one crystallite [20].

FTIR spectra of undoped and Cr-doped ZnO nanoparticles carried out in the wave number range 2000 to 400 cm^{-1} is shown in Fig. 7. FTIR measurements were done using KBr method at RT. According to these spectra, the absorption significant band at 448 and 530 cm^{-1} is showed to the characteristic stretching of Zn-O and Cr-O bond [21]. Peak located at 880 cm^{-1} are assigned to C-H. The peak located at 3435 cm^{-1} assigned to the stretching mode of O-H group, which reveals the presence of a small amount of water absorbed by the ZnO nanostructure. Absorption Stretching modes at 1460 and 1626 cm^{-1} are due to C-O and C=O. The peak located at 2926 cm^{-1} is due to asymmetric C-H bonds [22]. It is clear that the given FTIR spectra showing blue shift, which is credited to optical phonon confinement of nanostructures.

The magnetic properties of the pure ZnO and Cr doping ZnO samples were studied in terms of the vibrating sample magnetometer model (VSM-9600M-1, USA). The measurements were done at room temperature in a maximum applied field of 15 kOe. For technological application of nanocrystal semiconducting materials, it is very important to study their magnetic properties.

It is known that ZnO is nonmagnetic and Cr metal is paramagnetic at high temperature. The only ferromagnetic chromium dioxide is CrO_2 with a T_C of 386 K. The XRD pattern displayed that no phase of CrO_2 were found, thus, the Cr doped ZnO samples are expected to be free of ferromagnetic precipitates. However, the Cr-doped ZnO nanoparticle samples display obviously hysteresis loop at room temperature (M–H curve) as shown in Fig. 5, which demonstrates that the Cr-doped ZnO nanoparticles have good ferromagnetic property at room temperature.

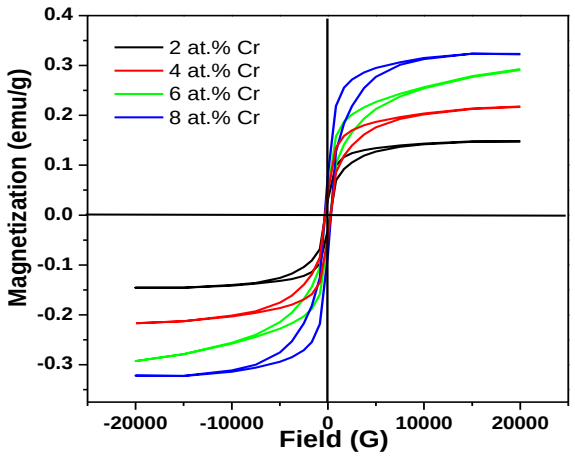

Fig. 8. Magnetization loops of the $Zn_{1-x}Cr_xO$ (x = 0.02, 0.04, 0.06 and 0.08) films measured at 300 K.

The magnetization (M) versus the magnetic field (H) measured at room temperature is shown in Fig 8. The magnetization is plotted as a function of magnetic field for different doping concentrations. All of the Cr-doped ZnO nanoparticles exhibit ferromagnetic behavior. The saturation magnetizations (Ms) of the Cr-doped ZnO nanoparticles varied in the range of 0.3219, 0.2909, 0.2176 and 0.1470 emu/g. The appearance of ferromagnetism in Cr-doped ZnO nanoparticles may attributed to two factors, the first is due to the increasing of the number of imperfection and vacancies of oxygen [23, 24, 25]; the second is due to the exchange interactions between Cr ions and O ions spin moments, for instance, Chu et al. predicted that most of the magnetic moment is induced by Cr 3d and O 2p spin moments through the theoretical calculations [26, 27].

4 Conclusions

Both undoped and Cr doped ZnO nanoparticles with composition of $Zn_{1-x}Cr_xO$ ((x = 0, 0.02, 0.04, 0.06 and 0.08) were synthesized using co-precipitation method. $Zn_{1-x}Cr_xO$ nanoparicles were characterized by TGA, EDAX, XRD, FTIR and VSM. The XRD patterns showed the formation of a wurtzite structure in the Cr-doped ZnO. characterizations of $Zn_{1-x}Cr_xO$ nanoparticles confirm that the Cr ions had taken the place of the Zn ions with +3 valence state in ZnO lattice, and the Cr-doping could restrain the growth of the crystal lattice. Williamson-Hall(W-H) analysis were used for determination both crystallize size and lattice strain. The results show that the crystallite size decreases with increasing Cr content but the lattice strain increases. The decrease in crystallite size and increase in lattice strain may be observed due to the replacement of Zn^{2+} ions by Cr^{3+} ions. The measured magnetic properties display that the Cr-doped ZnO nanoparticle are ferromagnetic with a well- defined hysteresis at room temperature. In addition, the remnant magnetization increase with increasing doping concentrations. The appearance of ferromagnetism in Cr-doped ZnO nanoparticles may attributed to two factors, the

first is due to the increasing of the number of defects and oxygen vacancies the second is due to the exchange interactions between Cr ions and O ions spin moments.

References

[1] J.M.D. Coey, M. Venkatesan, C.B. Fitzgerald, Nature Mater. 4 (2005) 173_179.

[2] T. Miyazaki, S. Yamasaki, Appl. Phys. Lett. 86 (2005) 261910-2.

[3] J J Liu, K Wang, M H Yu and W L Zhou J. Appl. Phys. 102 024301 (2007)

[4] E. R. Shaaban, M. El-Hagary, M. Emam-Ismail, A. Matar, I. S. Yahia, *Materials Science and Engineering B* 178 (2013) 183-189.

[5] H. Munekata, H. Ohno, S. von Molnar, and et al, Phys. Rev. Lett. 63, 1849 (1989).

[6] E. L. Nagaev, Physics of Magnetic Semiconductors (MIR moscow, 1983).

[7] D. J. Craik, Magnetic Oxides (Wiley New York, 1975).

[8] H. Ohno, Science 281, 951 (1998).

[9] H. Ohno, A. Shen, F. Matsukura, and et al, Appl. Phys. Lett. 69, 363 (1996).

[10] R Janisch, P Gopal and N A Spaldin J. Phys.: Condens. Matter. 17 R657 (2005).

[11] E. R. Shaaban, M. A. Kaid and M. G. S. Ali, *J. Alloys Compd.* **613** (2014) 324-329.

[12] H Wang et al. Nanotechnology 17 4312 (2006)

[13] Priya Gopal and Nicola A Spaldin Phys. Rev. B 74 094418 (2006)

[14] K Ueda, H Tabata and T Kawai Appl. Phys. Lett. 79 988 (2001)

[15] Z Jin et al. Appl. Phys. Lett. 78 3824 (2001)

[16] B K Roberts, A B Pakhomov, V S Shutthanandan and K M Krishnan J. Appl. Phys. 97 10D310 (2005)

[17] Y Liu et al. J. Solid State Chem. 184 1273 (2011)

[18] E. R. Shaaban, Ishu Kansal, S. H. Mohamed and J. M. F. Ferreira, *Physica B: Condensed matter* 404**,** 3571(2009).

[19] G. K. Williamson, W. H. Hall, X-ray line broadening from filed aluminum and wolfram, Acta Metall.1(1) (1953) 22–31.

[20] E. R. Shaaban, *J. Alloys Compd* 563 (2013) 274-279.

[21] Esparza M., Paredes R., Martinez A.G., Couto G., Loredo S., Luisa M., Velez F. and Dominguez O, Material Science and Application, Vol. 2, pp.1584, 2011.

[22] Vafaee M. and Sasani M.G., "Preparation and characterization of ZnO nanoparticles by novel sol-gel route" Materials Letters, Vol. 61, pp. 3265-3268, 2007.

[23] Q. Yan, J. Z. Chen, M. J. Tu, J. Rare Earth 21 (2003) 142.

[24] G.Z. Xing, J.B. Yi, D.D. Wang, L. Liao, T. Yu, Z.X. Shen, C.H.A. Huan, T.C. Sum, J. Ding, T.Wu, Phys. Rev. B 79 (2009) 174406.

[25] G.Z. Xing, J.B. Yi, J.G. Tao, T. Liu, L.M. Wong, Z. Zhang, G.P. Li, S.J. Wang, J. Ding, T.C. Sum, C.H.A. Huan, T.Wu, Adv. Mater. 20 (2008) 3521.

[26] D.W. Chu, Y.P. Zeng, D.L. Jiang, Solid State Commun. 143 (2007) 308.

[27] H. Liu, X. Zhang, L. Li, Y.X. Wang, K.H. Gao, Z.Q. Li, R.K. Zheng, S.P. Ringer, B. Zhang, X.X. Zhang, Appl. Phys. Lett. 91 (2007) 072511.